Title Page

Development and characterization of a ^{68}Ga-labeled A20FMDV2 peptide probe for the PET imaging of αvβ6 integrin-positive pancreatic ductal adenocarcinoma

Takashi Ui[a], Masashi Ueda[a], Yusuke Higaki[a], Shinichiro Kamino[a,1], Kohei Sano[b,2], Hiroyuki Kimura[b,3], Hideo Saji[b], Shuichi Enomoto[c]

[a] Graduate School of Medicine, Dentistry, and Pharmaceutical Sciences, Okayama University, 1-1-1 Tsushima-naka, Kita-ku, Okayama 700-8530, Japan.

[b] Graduate School of Pharmaceutical Sciences, Kyoto University, 46-29 Yoshida Shimoadachi-cho, Sakyo-ku, Kyoto 606-8501, Japan.

[c] RIKEN Center for Life Science Technologies, 6-7-3 Minatojima-minamimachi, Chuo-ku, Kobe 650-0047, Japan.

[1] Present address: School of Pharmaceutical Sciences, Aichi Gakuin University, Nagoya 464-8650, Japan.

[2] Present address: Department of Biophysical Chemistry, Kobe Pharmaceutical University, Kobe 658-8558, Japan.

[3] Present address: Department of Analytical and Bioinorganic Chemistry, Kyoto Pharmaceutical University, Kyoto 607-8414, Japan.

Corresponding author:

Masashi Ueda, Ph.D.

Department of Biofunction Imaging Analysis

Graduate School of Medicine, Dentistry, and Pharmaceutical Sciences

Okayama University

1-1-1 Tsushima-naka, Kita-ku, Okayama 700-8530, Japan

E-mail: mueda@cc.okayama-u.ac.jp

Abbreviations:

^{18}F-FDG, 2-deoxy-2-fluoro-^{18}F-D-glucopyranose; NOTA, 1,4,7-triazacyclononane-1,4,7-triacetic acid; PDAC, pancreatic ductal adenocarcinoma; PET, positron emission tomography

Abstract

Pancreatic ductal adenocarcinoma (PDAC) is known to be one of the most lethal cancers. Since the majority of patients are diagnosed at an advanced stage, development of a detection method for PDAC at an earlier stage of disease progression is strongly desirable. Integrin $\alpha_V\beta6$ is a promising target for early PDAC detection because its expression increases during precancerous changes. The present study aimed to develop an imaging probe for positron emission tomography (PET) which targets $\alpha_V\beta6$ integrin-positive PDAC. We selected A20FMDV2 peptide, which binds specifically to $\alpha v\beta6$ integrin, as a probe scaffold, and ^{68}Ga as a radioisotope. A20FMDV2 peptide has not been previously labeled with ^{68}Ga. A cysteine residue was introduced to the N-terminus of the probe at a site-specific conjugation of maleimide-NOTA (mal-NOTA) chelate. Different numbers of glycine residues were also introduced between cysteine and the A20FMDV2 sequence as a spacer in order to reduce the steric hindrance of the mal-NOTA on the binding probe to $\alpha V\beta6$ integrin. In vitro, the competitive binding assay revealed that probes containing a 6-glycine linker ([^{nat}Ga]CG6 and [^{nat}Ga]Ac-CG6) showed high affinity to $\alpha V\beta6$ integrin. Both probes could be labeled by $^{67/68}$Ga with high radiochemical yield (>50%) and purity (>98%). On biodistribution analysis, [^{67}Ga]Ac-CG6 showed higher tumor accumulation, faster blood clearance, and lower accumulation in the surrounding organs of pancreas than did [^{67}Ga]CG6. The $\alpha_V\beta6$ integrin-positive xenografts were clearly visualized by PET imaging with [^{68}Ga]Ac-CG6. The intratumoral distribution of [^{68}Ga]Ac-CG6 coincided with the $\alpha_V\beta6$ integrin-positive regions detected by immunohistochemistry.

Thus, [^{68}Ga]Ac-CG6 is a useful peptide probe for the imaging of $\alpha_V\beta6$ integrin in PDAC.

1. Introduction

Pancreatic ductal adenocarcinoma (PDAC) is known to be one of the most lethal cancers. As early-stage PDAC is minimally symptomatic, the majority of patients are diagnosed at advanced stages and are not eligible for surgical resection. PDAC also shows resistance to chemotherapy and radiotherapy. The 5-year survival rate for PDAC patients averages 5-8% and has not changed over the past 4 decades.[1-4] Therefore, development of a detection method for PDAC at an earlier stage of disease progression is strongly desirable.

There has been a recent focus on in vivo molecular imaging techniques that detect PDAC at an early, curable stage.[1, 3] The nuclear medicine technique of molecular imaging is one of these promising methods of diagnosis, because it can noninvasively obtain functional information about a living body, with high sensitivity. Worldwide, one of the most used radiopharmaceuticals for cancer detection in nuclear medicine is 2-deoxy-2-fluoro-^{18}F-D-glucopyranose (^{18}F-FDG). However, the effectiveness of ^{18}F-FDG-PET has been limited for PDAC, due to its susceptibility to false positives and false negatives in this setting.[1, 5] Thus, novel and more suitable radioactive probes are necessary for the diagnosis of PDAC.

Integrin αvβ6 mediates and modulates various cellular functions such as adhesion, migration, proliferation, invasion, and survival by binding to various ligands. In many cancers, including PDAC, the expression of αvβ6 integrin is upregulated. It is well known that αvβ6 integrin not only serves as a poor prognostic indicator, but is also involved in tumor proliferation, invasion,

and treatment-resistance.[6, 7] Although αvβ6 integrin is expressed at undetectable level in a normal pancreas, its levels gradually increase as the associated pathology progresses from a premalignant lesion to PDAC.[8] Approximately 94% of PDAC patients strongly express αvβ6 integrin.[9] The expression level of αvβ6 integrin in PDAC is significantly higher than that of inflammatory disorders of the pancreas.[10] Taking this into account, αvβ6 integrin is one of the most promising targets for the detection of PDAC at an early stage.

Several radioactive probes which target αvβ6 integrin have already been developed.[11-22] A20FMDV2 peptide has been used for many probes as a parent scaffold and an ^{18}F-labeled A20FMDV2 derivative has successfully visualized various tumors, including the lung metastasis of PDAC, in a First-in-Human study.[23] A20FMDV2 peptide has been labeled with ^{18}F and ^{64}Cu for PET imaging.[16, 19, 21-23] Among positron emitters, ^{68}Ga can be readily obtained from a ^{68}Ge/^{68}Ga generator and thus, ^{68}Ga-labeled probes may be cost-effective and generalizable, because there is no requirement for cyclotron use. The half-life of ^{68}Ga is 68 min, resulting in less radiation exposure compared to positron emitters with long half-lives, such as ^{64}Cu. However, A20FMDV2 peptide has never been labeled with ^{68}Ga.

In the present study, we aimed to develop a ^{68}Ga-labeled A20FMDV2 peptide probe for the PET imaging of αvβ6 integrin-positive PDAC. We introduced a cysteine residue to the N-terminus of A20FMDV2 to site-specific conjugation of maleimide-NOTA (mal-NOTA) chelate. Moreover, different numbers of glycine residues were also introduced between cysteine and the A20FMDV2

sequence as a spacer, in order to reduce the steric hindrance of the mal-NOTA on the binding probe to αVβ6 integrin. The competitive binding assay in vitro revealed that 6 glycine residues were the best spacer length. Acetylation at the N-terminus increased the stability of the probe in plasma and provided a favorable profile during biodistribution. As a result, αVβ6 integrin-positive xenografts were clearly visualized by PET imaging with Ac-Cys(mal-NOTA-^{68}Ga)-Gly6-A20FMDV2 ([^{68}Ga]Ac-CG6) probe, and [^{68}Ga]Ac-CG6 would be a useful probe for the in vivo detection of αVβ6 integrin-positive PDAC.

2. Materials and Methods

2.1. Probe design and peptide synthesis

According to our previous study, the N-terminal side of A20FMDV2 could be labeled by [^{123}I]iodophenylmaleimide without hampering its affinity to αVβ6 integrin.[18] A cysteine residue was therefore introduced to the N-terminus of A20FMDV2 to site-specific conjugation of the mal-NOTA chelate. To reduce the effect of steric hindrance of the mal-NOTA on binding to αVβ6 integrin, different numbers (1, 4, 6, and 8) of glycine residues were introduced between cysteine and the A20FMDV2 sequence as a spacer. Acetylation at the N-terminus was also performed, particularly in the case of the 6-glycine-containing probe. The probes evaluated in this study are shown in Table 1.

The Rink amide MBHA Resin and 9-fluorenylmethyloxycarbonyl (Fmoc)-protected amino acids were purchased from Watanabe Chemical Industries, Ltd. (Hiroshima, Japan). All of the peptides utilized in this study were synthesized via Fmoc solid-phase peptide synthesis using an automated peptide synthesizer (PSSM-8; Shimadzu Corporation, Kyoto, Japan) according to a previously described method.[24] The crude peptides were purified by reverse-phase high-performance liquid chromatography (HPLC) equipped with a 5C$_{18}$-AR-II column (10 × 250 mm; Nacalai Tesque, Inc., Kyoto, Japan).

The purified peptides were incubated with maleimide-NOTA (CheMatech, Dijon, France) in a total volume of 100 μL of 0.2 M ammonium acetate buffer (pH 6.5) at 25°C for 60 min. The reaction solution was purified by HPLC to obtain NOTA-conjugated peptides. The NOTA-conjugated peptides were dissolved in 100 μL of 0.2 M sodium acetate buffer (pH 4.0), GaCl$_3$ (Nacalai Tesque, Inc.) was dissolved in 50 μL of 1 M HEPES buffer (pH 6.0), and both solutions were incubated at 25°C for 60 min. The reaction solution was purified by HPLC to obtain non-radioactive authentic probes.

The identities were determined by analytical HPLC (5C$_{18}$-AR-II column [4.6 × 150 mm]; Nacalai Tesque, Inc.; a linear gradient of 0.1% aqueous trifluoroacetic acid (TFA) and acetonitrile from 8:2 to 6:4 over 20 min, 1.0 mL/min; wave length, 220 nm) and electrospray ionization mass spectroscopy (API 4000; SCIEX, Framingham, MA). Data relating to peptide mass are summarized in Table S1.

2.2. Cells and Cell culture

AsPC-1 and MIA PaCa-2 human pancreatic carcinoma cells were obtained from the European Collection of Authenticated Cell Cultures and the Japanese Collection of Research Bioresources Cell Bank, respectively. Both cell lines were maintained in Dulbecco's modified Eagle's medium (Nissui Pharmaceutical, Tokyo, Japan) supplemented with 10% fetal bovine serum, penicillin (100 units/mL), and streptomycin (100 μg/mL). The cells were incubated at 37°C in a well-humidified incubator with 5% CO_2 and 95% air.

2.3. Competitive binding assay

The affinity of the probes was evaluated by a competitive binding assay using ^{125}I-IFMDV2 as a radioligand. Detailed methods of ^{125}I-IFMDV2 preparation and binding assay were described previously.[18]

2.4. Radiolabeling

Gallium-67 chloride (^{67}GaCl$_3$) was kindly supplied by FUJIFILM RI Pharma Co., Ltd. (Tokyo, Japan). The NOTA-conjugated peptides (3-40 μg) were dissolved in 100 μL of 0.2 M sodium acetate buffer (pH 4.0), and the ^{67}GaCl$_3$ (2-87 MBq) was dissolved in 50 μL of 1 M HEPES buffer (pH 6.0). Both solutions were incubated at 75°C for 15 min. The reaction solution was

purified by HPLC using analytical HPLC conditions.

Gallium-68 chloride (^{68}GaCl$_3$) was obtained from a ^{68}Ge/^{68}Ga generator (ITG Isotope Technologies Garching GmbH, Munchen, Germany) by use of 0.05 M HCl as an eluent. The NOTA-conjugated peptides (5-20 µg) were dissolved in 80 µL of 1.5 M sodium acetate aqueous solution and mixed with ^{68}GaCl$_3$ (337-503 MBq) in 2.0 mL of 0.05 M HCl. The mixture was incubated at 75°C for 15 min and was then applied to Sep-Pak C18 Cartridges (Waters Corporation, Milford, MA). After the cartridges were washed twice using 500 µL of water, the ^{68}Ga-labeled peptides were eluted 3 times using 500 µL of a mixture of 0.1% aqueous TFA and methanol (6:4). The purity of the probe was checked by HPLC (5C$_{18}$-AR-II column [4.6 × 150 mm]; 0.1% aqueous TFA:acetonitrile = 73:27; 1.0 mL/min; wave length, 230 nm).

After the removal of the organic solvent, the probes were used for further experiments.

2.5. In vitro stability

Animal experiments were performed in accordance with the guidelines of the Okayama University and Kyoto University Animal Care Committees. The experimental procedures performed were approved by both committees. Male ICR mice at 6 weeks of age were purchased from Japan SLC, Inc (Hamamatsu, Japan). Under 2.5% isoflurane anesthesia, blood was withdrawn from the hearts of the mice using heparinized syringes and was centrifuged (1,000 × *g*) at 4°C for 5 min to obtain plasma. ^{67}Ga-labeled peptides (150 µL) were incubated in mouse plasma (300 µL) at 37°C,

and 50 μL of the samples were collected at selected time points. To remove proteins from the plasma, the samples were mixed with 100 μL of methanol and were centrifuged (1,000 × *g*) at 4°C for 5 min. After filtration, the eluents were analyzed by HPLC as described above.

2.6. Animal model

Male severe combined immunodeficiency mice (C.B-17/Icr-scid/scid Jcl) at 5 weeks of age were purchased from CLEA Japan, Inc (Tokyo, Japan). Models of AsPC-1 and MIA PaCa-2 tumors were prepared according to a previously described method.[18]

2.7. Biodistribution

^{67}Ga-labeled peptides (100 kBq) were injected into tumor-bearing mice (n = 3-4) via the tail vein. The specific activities of [^{67}Ga]CG6 and [^{67}Ga]Ac-CG6 were 3.88 and 1.14 GBq/μmol, respectively. At a post-injection interval of 10, 60, and 120 min, mice were dissected and whole organs were immediately obtained and weighed, and their radioactivity was measured. The results were expressed as the percent injected dose per gram of tissue (%ID/g).

To confirm that [^{67}Ga]Ac-CG6 was specifically bound to αVβ6 integrin in vivo, a blocking study was conducted. Phosphate-buffered saline (PBS) alone or PBS solution of 20 nmol of A20FMDV2 were injected into the tumor-bearing mice (n = 3–4) via the tail vein, and 5 min later, [^{67}Ga]Ac-CG6 (100 kBq; specific activity: 0.42 GBq/μmol) was also injected via the tail vein.

Biodistribution was determined 1 h after the injection of [^{67}Ga]Ac-CG6 following the aforementioned method.

2.8. PET/X-ray computed tomography (CT) imaging

Tumor-bearing mice (n = 2) were intravenously injected with 200 μL of [^{68}Ga]Ac-CG6 (9.88 or 20.4 MBq; specific activity: 44.2 GBq/μmol). At 52 min after injection, a 15-min PET scan followed by a 5-min CT scan were performed using Triumph LabPET12/SPECT4/CT (TriFoil Imaging Inc., Chatsworth, CA, USA) under 2.5% isoflurane anesthesia.[25] Parameters for both scans and for image reconstruction were adjusted as per those used in a previous report.[26] After PET/CT imaging, the mice were killed, and each tumor was removed and frozen for further analysis.

2.9. Autoradiography and histological analysis

After PET/CT imaging, 20-μm-thick sections and adjacent 4-μm-thick sections of frozen tumors were prepared with a cryomicrotome (CM1900 Cryostat; Leica Microsystems, Wetzlar, Germany). The 20-μm-thick sections were exposed to an imaging plate (BAS-SR; Fuji Photo Film, Tokyo, Japan) for 1 h and autoradiograms of these sections were obtained using a BAS5000 scanner (Fuji Photo Film).[27]

The 4-μm-thick sections were incubated with anti-integrin β6 mouse mAb (Millipore, Burlington, USA) for 12 h at 4°C followed by anti-mouse IgG, horseradish peroxidase-linked whole

12

antibody (GE Healthcare, Boston, USA) for 2 h at room temperature. Finally, DAB staining and counterstaining with hematoxylin were performed.

2.10. Statistical Analyses

Comparisons between the 2 groups were made using the Mann-Whitney *U*-test. A *P* value of <0.05 was considered statistically significant.

3. Results

3.1. Binding affinity evaluation

The affinity of each probe for αVβ6 integrin was evaluated by a competitive binding assay using αVβ6-integrin-positive cells. The calculated Ki value of each probe is shown in Table 1. Of the probes used, the 6-glycine-containing probes ([^{nat}Ga]CG6 and [^{nat}Ga]Ac-CG6) showed the highest affinity. The Ki value of non-modified A20FMDV2 was 4.2 ± 1.4 nM and both the probes exhibited a comparable affinity to the parent peptide. However, the affinity of 1-, 4-, or 8-glycine-containing probes were approximately 40–150 folds lower compared to the parent peptide.

3.2. Radiolabeling

The radiolabeled peptides could not be separately obtained from the corresponding precursor peptides. ^{67}Ga-labeling ($[^{67}$Ga]CG6 and $[^{67}$Ga]Ac-CG6) was performed, resulting in a radiochemical yield of 32-83%. The radiochemical yield of $[^{68}$Ga]Ac-CG6 were 56-84%. The radiochemical purity of each probe was >95% (Fig. S1).

3.3. In vitro stability

The stability of $[^{67}$Ga]CG6 and $[^{67}$Ga]Ac-CG6 in mouse plasma was analyzed by HPLC. The recovery of radioactivity from the HPLC column was 101.2 ± 4.2% in the case of $[^{67}$Ga]CG6 and 97.9 ± 7.6% in the case of $[^{67}$Ga]Ac-CG6. The temporal changes in intact forms of each probe are shown in Figure 1. Although both probes showed high stability (> 80%) in mouse plasma up to 2-h incubation, the stability of $[^{67}$Ga]Ac-CG6 was significantly higher than that of $[^{67}$Ga]CG6 at 1 h ($[^{67}$Ga]CG6: 89.3 ± 0.3%, $[^{67}$Ga]Ac-CG6: 94.3 ± 0.7%, $P < 0.05$) and 2 h ($[^{67}$Ga]CG6: 81.7 ± 1.1%, $[^{67}$Ga]Ac-CG6: 89.3 ± 0.5%, $P < 0.05$).

3.4. Biodistribution

The biodistribution of $[^{67}$Ga]CG6 and $[^{67}$Ga]Ac-CG6 was evaluated in mice bearing AsPC-1 (αVβ6 integrin positive) and MIA PaCa-2 (αVβ6 integrin negative) xenografts. The results are shown in Table 2. Both probes showed the accumulation in the kidneys. Moderate accumulation of both probes was observed in the stomach and intestine, both αVβ6-integrin-positive organs.

[^{67}Ga]CG6 showed higher accumulation in the AsPC-1 xenograft compared to blood and MIA PaCa-2 xenograft at 60 or 120 min after injection. The ratios of AcPC-1-to-blood and AsPC-1-to-MIA PaCa-2 were around 2-3. However, [^{67}Ga]CG6 also accumulated in the liver and spleen at a level similar to that of the AsPC-1 xenograft. On the other hand, the accumulation of [^{67}Ga]Ac-CG6 in the liver and spleen was significantly lower than that of [^{67}Ga]CG6. Moreover, there was significantly more accumulation of [^{67}Ga]Ac-CG6 than [^{67}Ga]CG6 in the AsPC-1 xenograft. Levels of accumulation in the blood and MIA PaCa-2 xenograft were lower for [^{67}Ga]CG6, resulting in the ratios of AcPC-1-to-blood and AsPC-1-to-MIA PaCa-2 increasing to 5-7.

Figure 2 shows the results of the in vivo blocking study. The pretreatment of the excess amount of A20FMDV2 decreased in the accumulation of [^{67}Ga]Ac-CG6 in the AsPC-1 xenograft significantly by approximately 40%. However, the radioactivity in the blood and MIA PaCa-2 xenograft were at similar levels in both the groups.

3.5. PET/CT imaging

Because [^{67}Ga]Ac-CG6 showed more favorable in vivo property than [^{67}Ga]CG6, PET imaging with [^{68}Ga]Ac-CG6 was performed. The AsPC-1 xenograft was clearly visualized at 1 h post-injection of [^{68}Ga]Ac-CG6, while little radioactivity accumulated in the MIA PaCa-2 xenograft (Fig. 3).

15

3.6. Autoradiography and histological analysis

To prove the specific accumulation of [^{68}Ga]Ac-CG6 in areas where αVβ6 integrin is present in vivo, we compared the radioactivity accumulation areas to the areas where β6 integrin was expressed in the tumors. Figure 4 represents the autoradiograms and images of the immunohistochemical staining of each tumor section. On immunohistochemistry, β6 integrin was strongly expressed in the marginal regions of the AsPC-1 xenograft but was hardly detected in the MIA PaCa-2 xenograft. Areas of [^{68}Ga]Ac-CG6 accumulation corresponded to β6-integrin-positive areas.

4. Discussion

In this study, we developed ^{68}Ga-labeled A20FMDV2-based probes for the PET evaluation of αVβ6 integrin expression. We discovered that the suitable length of the spacer between the peptide and NOTA chelate was 6 glycine residues. N-terminal acetylation did not impair probe affinity but did increase probe stability. On biodistribution analysis, although both [^{67}Ga]CG6 and [^{67}Ga]Ac-CG6 showed higher levels of accumulation in the αVβ6 integrin-positive xenografts compared to the negative xenografts, the tumoral accumulation of [^{67}Ga]Ac-CG6 were greater than that of [^{67}Ga]CG6. The tumor-to-blood and tumor-to-adjacent organ accumulation ratios were also

greater for [^{67}Ga]Ac-CG6 than [^{67}Ga]CG6. [^{68}Ga]Ac-CG6 clearly visualized the αVβ6 integrin-positive xenografts in vivo, and the probe-accumulated areas coincided with the areas of β6-integrin expression. These findings indicate that [^{68}Ga]Ac-CG6 would be a useful probe for the detection of αVβ6 integrin-positive PDAC on PET imaging.

N-acetylation was reported to provide resistance against the enzymatic cleavage of a peptide.[28] In accordance with previous findings, the stability of [^{67}Ga]Ac-CG6 in mouse plasma was significantly greater than that of [^{67}Ga]CG6. Moreover, [^{67}Ga]Ac-CG6 showed a significantly reduced uptake in the liver, spleen, and kidneys compared to [^{67}Ga]CG6. A20FMDV2 peptide contains 3 basic amino acids and 1 acidic amino acid, thus the theoretical net charge of [^{67}Ga]CG6 is +3 and [^{67}Ga]Ac-CG6 is +2. It was reported that increased positive charges triggers phagocytosis by macrophages in the reticuloendothelial system.[29] Therefore, the reduced uptake in the liver and spleen could be partly attributable to a decrease in the net charge of the probe. These findings are consistent with the previous reported finding that the N-acetylation of a divalent probe, with a decrease in the net charge of the probe +4 to +2, could reduce non-specific accumulation in the liver and kidneys.[30] As the liver and spleen are anatomically adjacent to the pancreas, low accumulation in those organs is a desirable feature of a PDAC imaging probe. [^{67}Ga]Ac-CG6 displayed high tumor-to-liver and -spleen ratios with values greater than 7.

Of those examined in this study, the best spacer length between the peptide and the NOTA chelate was found to be 6 glycine residues. Radiolabeling of A20FMDV2 peptide was generally

performed in 2 ways. The first was the direct conjugation of a prosthetic group or a chelate to the N-terminal of the peptide,[18, 22, 31] and the second was their introduction via a polyethylene glycol (PEG) linker.[16, 19, 21, 32, 33] The length of the PEG varied from 7 to 56. Since PEG is known to be flexible, it may be helpful to avoid steric hindrance between the αVβ6 integrin and the prosthetic group or chelate. To our surprise, the [^{nat}Ga]CG showed approximately 25- and 50-fold less affinity compared to [^{nat}Ga]Ac-CG6 and [^{nat}Ga]CG6, respectively. Conjugation of iodophenylmaleimide to CG-A20FMDV2 maintained its affinity to αVβ6 integrin, and the αVβ6 integrin-positive xenograft was clearly visualized in vivo by SPECT imaging.[18] Therefore, the structure of maleimide-NOTA may cause this decrease in its binding affinity to αVβ6 integrin. Computational sciences such as docking simulations of the probes and of αVβ6 integrin would solve the question of why 6-glycine, not 1-glycine, linker probes showed high binding affinity. However, the crystal structure of αVβ6 integrin has never been determined in a protein data bank.

To date, one ^{18}F-labeled PEGylated A20FMDV2 peptide probe ([^{18}F]αvβ6-BP) has been successfully finished its First-in-Human study.[23] In preclinical evaluation, the accumulation of [^{18}F]αvβ6-BP in the αVβ6 integrin-positive xenografts, αVβ6 integrin-negative xenografts, blood, and liver at 1 hr after injection is 2.51, 0.35, 0.34, and 0.28 %ID/g, respectively. Although different tumor cells were used in the present study, the accumulation of [^{68}Ga]Ac-CG6 in those organs was mostly comparable at 1 hr after injection. However, one drawback of [^{68}Ga]Ac-CG6 was its high non-specific accumulation and retention in the kidneys. At 1 hr after injection, 22.88 %ID/g of

[^{18}F]αvβ6-BP had accumulated in the kidneys, a result which was 4-fold lower than that of [^{68}Ga]Ac-CG6. It cleared in a time-dependent manner (7.87 %ID/g at 4 hr). In contrast, the accumulation of [^{68}Ga]Ac-CG6 in the kidneys remained at a level greater than 75 %ID/g at 2 h post-injection. Therefore, further structural modification, such as the incorporation of renal brush border enzyme-cleavable linkers,[34] will be required to reduce the renal retention of [^{68}Ga]Ac-CG6.

There is another probe containing a peptide sequence different to that of A20FMDV2 which is eligible for a First-in-Human study.[35] Altmann *et al*. identified several αVβ6 integrin-binding peptides via a phage display technique and radiolabeled one of them, named SFITGv6, for the noninvasive detection of head and neck squamous cell carcinoma. In their experiment, the affinity of A20FMDV2 was approximately 5-fold higher than that of SFITGv6. However, the accumulation of ^{177}Lu-DOTA-SFITGv6 in the αVβ6 integrin-positive xenografts was of approximately 4 %ID/g at 1 hr after injection and was greater than [^{68}Ga]Ac-CG6, although the evaluation was performed using different cell lines. It also showed a greater tumor-to-blood ratio than [^{68}Ga]Ac-CG6, which might be attributable to shorter peptide length, 10-mer, of SFITGv6.

Conclusion

By incorporating 6 glycine residues between A20FMDV2 peptide and NOTA-conjugated cysteine, we can perform ^{68}Ga labeling while maintaining its binding affinity to αvβ6 integrin.

N-acetylation not only provided an increase in the stability of the probe in plasma, but also resulted in favorable biodistribution profile, i.e., an increase in tumor uptake and a decrease in nonspecific accumulation in the liver, spleen, and kidneys. [^{68}Ga]Ac-CG6 allowed clear visualization of αvβ6 integrin-positive xenografts in PET imaging. These findings indicate that [^{68}Ga]Ac-CG6 would be a useful probe for the non-invasive detection of PDAC.

Acknowledgments

References

1.   Singhi AD, Koay EJ, Chari ST, et al. Early Detection of Pancreatic Cancer: Opportunities and Challenges. *Gastroenterology.* 2019;156:2024-2040.

2.   Sun Q, Zhang B, Hu Q, et al. The impact of cancer-associated fibroblasts on major hallmarks of pancreatic cancer. *Theranostics.* 2018;8:5072-5087.

3.   Cornelissen B, Knight JC, Mukherjee S, et al. Translational molecular imaging in exocrine pancreatic cancer. *Eur J Nucl Med Mol Imaging.* 2018;45:2442-2455.

4.   Zhu H, Li T, Du Y, et al. Pancreatic cancer: challenges and opportunities. *BMC Med.* 2018;16:214.

5.   Strobel O, Buchler MW. Pancreatic cancer: FDG-PET is not useful in early pancreatic cancer diagnosis. *Nat Rev Gastroenterol Hepatol.* 2013;10:203-205.

6.   Koivisto L, Bi J, Hakkinen L, et al. Integrin alphavbeta6: Structure, function and role in health and disease. *Int J Biochem Cell Biol.* 2018;99:186-196.

7.   Niu J, Li Z. The roles of integrin alphavbeta6 in cancer. *Cancer Lett.* 2017;403:128-137.

8.   Hezel AF, Deshpande V, Zimmerman SM, et al. TGF-beta and alphavbeta6 integrin act in a common pathway to suppress pancreatic cancer progression. *Cancer Res.* 2012;72:4840-4845.

9.   Sipos B, Hahn D, Carceller A, et al. Immunohistochemical screening for beta6-integrin subunit expression in adenocarcinomas using a novel monoclonal antibody reveals strong up-regulation in pancreatic ductal adenocarcinomas in vivo and in vitro. *Histopathology.*

2004;45:226-236.

10.   Tummers WS, Farina-Sarasqueta A, Boonstra MC, et al. Selection of optimal molecular targets for tumor-specific imaging in pancreatic ductal adenocarcinoma. *Oncotarget.* 2017;8:56816-56828.

11.   Flechsig P, Lindner T, Loktev A, et al. PET/CT Imaging of NSCLC with a alphavbeta6 Integrin-Targeting Peptide. *Mol Imaging Biol.* 2019. doi: 10.1007/s11307-018-1296-6.

12.   Liu H, Gao L, Yu X, et al. Small-animal SPECT/CT imaging of cancer xenografts and pulmonary fibrosis using a ^{99m}Tc-labeled integrin alphavbeta6-targeting cyclic peptide with improved in vivo stability. *Biophys Rep.* 2018;4:254-264.

13.   Roesch S, Lindner T, Sauter M, et al. Comparison of the RGD Motif-Containing alphavbeta6 Integrin-Binding Peptides SFLAP3 and SFITGv6 for Diagnostic Application in HNSCC. *J Nucl Med.* 2018;59:1679-1685.

14.   White JB, Hu LY, Boucher DL, et al. ImmunoPET Imaging of alphavbeta6 Expression Using an Engineered Anti-alphavbeta6 Cys-diabody Site-Specifically Radiolabeled with Cu-64: Considerations for Optimal Imaging with Antibody Fragments. *Mol Imaging Biol.* 2018;20:103-113.

15.   Notni J, Reich D, Maltsev OV, et al. In Vivo PET Imaging of the Cancer Integrin alphavbeta6 Using ^{68}Ga-Labeled Cyclic RGD Nonapeptides. *J Nucl Med.* 2017;58:671-677.

16.   Hausner SH, Bauer N, Hu LY, et al. The Effect of Bi-Terminal PEGylation of an Integrin

alphavbeta6-Targeted [18]F Peptide on Pharmacokinetics and Tumor Uptake. *J Nucl Med.* 2015;56:784-790.

17. Liu Z, Liu H, Ma T, et al. Integrin alphavbeta6-Targeted SPECT Imaging for Pancreatic Cancer Detection. *J Nucl Med.* 2014;55:989-994.

18. Ueda M, Fukushima T, Ogawa K, et al. Synthesis and evaluation of a radioiodinated peptide probe targeting alphavbeta6 integrin for the detection of pancreatic ductal adenocarcinoma. *Biochem Biophys Res Commun.* 2014;445:661-666.

19. Hu LY, Bauer N, Knight LM, et al. Characterization and evaluation of ^{64}Cu-labeled A20FMDV2 conjugates for imaging the integrin alphavbeta 6. *Mol Imaging Biol.* 2014;16:567-577.

20. John AE, Luckett JC, Tatler AL, et al. Preclinical SPECT/CT imaging of alphavbeta6 integrins for molecular stratification of idiopathic pulmonary fibrosis. *J Nucl Med.* 2013;54:2146-2152.

21. Hausner SH, Abbey CK, Bold RJ, et al. Targeted in vivo imaging of integrin alphavbeta6 with an improved radiotracer and its relevance in a pancreatic tumor model. *Cancer Res.* 2009;69:5843-5850.

22. Hausner SH, DiCara D, Marik J, et al. Use of a peptide derived from foot-and-mouth disease virus for the noninvasive imaging of human cancer: generation and evaluation of 4-[^{18}F]fluorobenzoyl A20FMDV2 for in vivo imaging of integrin alphavbeta6 expression with positron emission tomography. *Cancer Res.* 2007;67:7833-7840.

23.   Hausner SH, Bold RJ, Cheuy LY, et al. Preclinical Development and First-in-Human Imaging of the Integrin alphavbeta6 with [^{18}F]alphavbeta6-Binding Peptide in Metastatic Carcinoma. *Clin Cancer Res.* 2019;25:1206-1215.

24.   Ueda M, Ogawa K, Miyano A, et al. Development of an oxygen-sensitive degradable peptide probe for the imaging of hypoxia-inducible factor-1-active regions in tumors. *Mol Imaging Biol.* 2013;15:713-721.

25.   Ueda M, Yamagami D, Watanabe K, et al. Histological and Nuclear Medical Comparison of Inflammation After Hemostasis with Non-Thermal Plasma and Thermal Coagulation. *Plasma Process Polym.* 2015;12:1338-1342.

26.   Ueda M, Hisada H, Temma T, et al. Gallium-68-labeled anti-HER2 single-chain Fv fragment: development and in vivo monitoring of HER2 expression. *Mol Imaging Biol.* 2015;17:102-110.

27.   Matsuura Y, Ueda M, Higaki Y, et al. Evaluation of the Relationship Between Cognitive Impairment, Glycometabolism, and Nicotinic Acetylcholine Receptor Deficits in a Mouse Model of Alzheimer's Disease. *Mol Imaging Biol.* 2019;21:519-528.

28.   Werle M, Bernkop-Schnurch A. Strategies to improve plasma half life time of peptide and protein drugs. *Amino Acids.* 2006;30:351-367.

29.   Xiao K, Li Y, Luo J, et al. The effect of surface charge on in vivo biodistribution of PEG-oligocholic acid based micellar nanoparticles. *Biomaterials.* 2011;32:3435-3446.

30.   Singh AN, McGuire MJ, Li S, et al. Dimerization of a phage-display selected peptide for imaging of alphavbeta6- integrin: two approaches to the multivalent effect. *Theranostics.* 2014;4:745-760.

31.   Saha A, Ellison D, Thomas GJ, et al. High-resolution in vivo imaging of breast cancer by targeting the pro-invasive integrin alphavbeta6. *J Pathol.* 2010;222:52-63.

32.   Hausner SH, Bauer N, Sutcliffe JL. In vitro and in vivo evaluation of the effects of aluminum [^{18}F]fluoride radiolabeling on an integrin alphavbeta6-specific peptide. *Nucl Med Biol.* 2014;41:43-50.

33.   Hausner SH, Carpenter RD, Bauer N, et al. Evaluation of an integrin alphavbeta6-specific peptide labeled with [^{18}F]fluorine by copper-free, strain-promoted click chemistry. *Nucl Med Biol.* 2013;40:233-239.

34.   Suzuki C, Uehara T, Kanazawa N, et al. Preferential Cleavage of a Tripeptide Linkage by Enzymes on Renal Brush Border Membrane To Reduce Renal Radioactivity Levels of Radiolabeled Antibody Fragments. *J Med Chem.* 2018;61:5257-5268.

35.   Altmann A, Sauter M, Roesch S, et al. Identification of a Novel ITGalphavbeta6-Binding Peptide Using Protein Separation and Phage Display. *Clin Cancer Res.* 2017;23:4170-4180.

Table 1. Ki values of the probes

Name	Ki (nM)
H-Cys(mal-NOTA-^{nat}Ga)-Gly-A20FMDV2-NH$_2$ ([^{nat}Ga]CG)	161 ± 59
H-Cys(mal-NOTA-^{nat}Ga)-Gly4-A20FMDV2-NH$_2$ ([^{nat}Ga]CG4)	633 ± 95
H-Cys(mal-NOTA-^{nat}Ga)-Gly6-A20FMDV2-NH$_2$ ([^{nat}Ga]CG6)	3.5 ± 0.3
Ac-Cys(mal-NOTA-^{nat}Ga)-Gly6-A20FMDV2-NH$_2$ ([^{nat}Ga]Ac-CG6)	6.6 ± 1.9
H-Cys(mal-NOTA-^{nat}Ga)-Gly8-A20FMDV2-NH$_2$ ([^{nat}Ga]CG8)	187 ± 64

Values are represented as the mean ± S.D., *n* = 3.

Table 2. Biodistribution of [^{67}Ga]CG6 and [^{67}Ga]Ac-CG6 in tumor-bearing mice

	10 min		60 min		120 min	
Organ	[^{67}Ga]CG6	[^{67}Ga]Ac-CG6	[^{67}Ga]CG6	[^{67}Ga]Ac-CG6	[^{67}Ga]CG6	[^{67}Ga]Ac-CG6
Blood	1.87 ± 0.35	0.77 ± 0.03*	0.58 ± 0.13	0.41 ± 0.04	0.44 ± 0.09	0.28 ± 0.03*
AsPC-1	2.23 ± 0.42	2.99 ± 0.32*	1.64 ± 0.25	2.23 ± 0.36*	1.11 ± 0.14	2.02 ± 0.22*
MIA PaCa-2	2.03, 2.14†	1.04 ± 0.13	0.65 ± 0.17	0.43 ± 0.06	0.53 ± 0.04	0.41 ± 0.16
Spleen	1.05 ± 0.45	0.26 ± 0.04*	1.07 ± 0.69	0.16 ± 0.04*	1.12 ± 0.55	0.14 ± 0.01*
Pancreas	3.70 ± 1.84	1.42 ± 0.08*	1.03 ± 0.31	0.69 ± 0.07	0.85 ± 0.25	0.61 ± 0.08
Liver	1.37 ± 0.60	0.40 ± 0.06*	0.97 ± 0.43	0.29 ± 0.05*	0.90 ± 058.	0.26 ± 0.03*
Intestine	8.74 ± 5.08	8.90 ± 0.74	5.90 ± 1.02	6.84 ± 0.90	5.48 ± 0.92	6.30 ± 0.38
Kidneys	102.95 ± 7.55	79.61 ± 6.88*	129.68 ± 21.03	81.11 ± 6.64*	123.51 ± 16.48	75.25 ± 9.45*
Stomach	13.63 ± 9.19	11.64 ± 2.68	14.08 ± 3.39	14.44 ± 4.40	10.12 ± 0.78	11.99 ± 0.96*
Heart	2.28 ± 0.79	3.52 ± 1.71	1.74 ± 0.24	1.51 ± 0.19	1.36 ± 0.19	1.44 ± 0.21
Lung	5.24 ± 2.33	3.48 ± 1.52	4.68 ± 1.38	3.83 ± 0.51	3.63 ± 0.80	3.41 ± 0.71
Muscle	1.57 ± 0.54	2.02 ± 0.13	1.65 ± 0.50	1.72 ± 0.25	1.77 ± 0.35	1.84 ± 0.28

Organ uptake values are expressed as percent injected dose per gram of tissue.

Values are represented as mean ± S.D., n = 3–4.

* indicates $P < 0.05$ vs. [^{67}Ga]CG6 at the same time point (Mann-Whitney U-test).

† Data of the two tumors is shown because MIA PaCa-2 cells did not engraft in 1 of 3 mice.
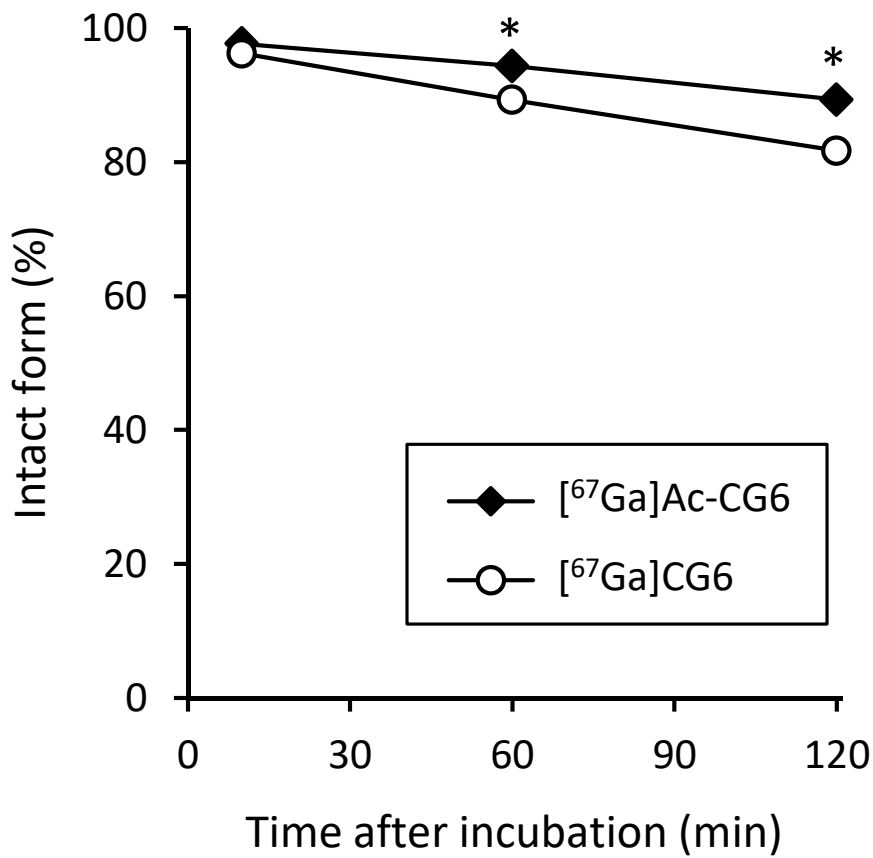
Figure 1

Fig. 1. *In vitro* stability of [^{67}Ga]CG6 and [^{67}Ga]Ac-CG6.

Each data point represents an average of 3 independent examinations. Each error bar represents the

standard deviation but it is too small to be seen. * indicates *P* < 0.05 (Mann–Whitney *U*-test).
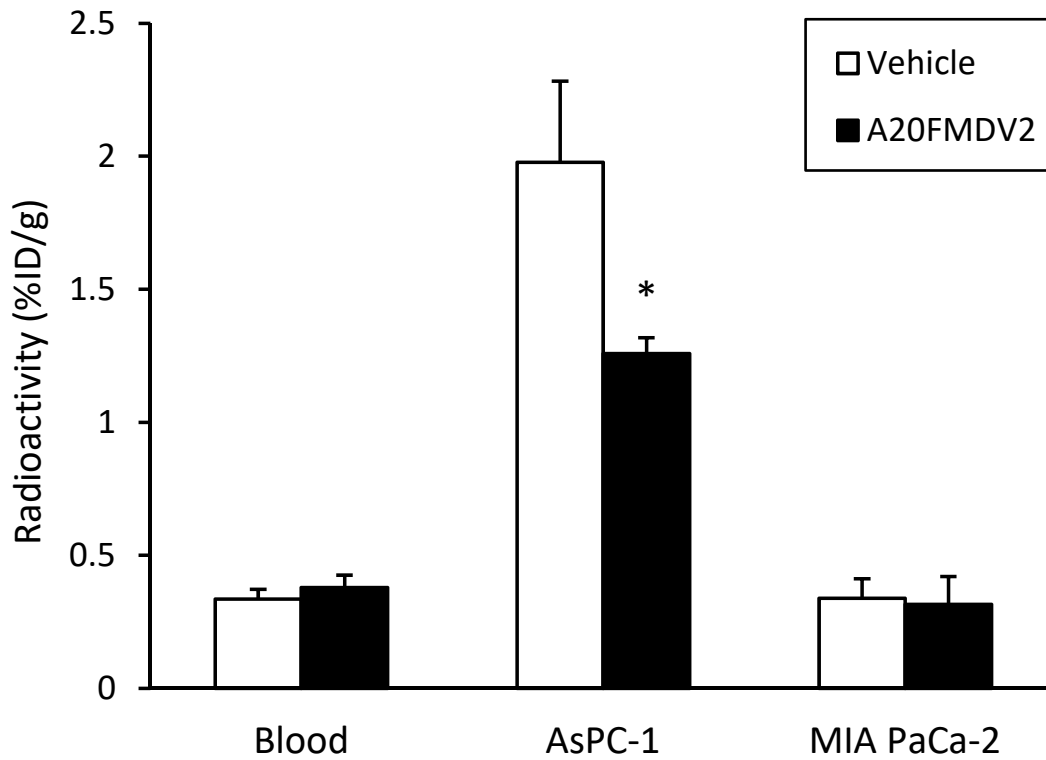
Figure 2

Fig. 2. Effects of A20FMDV2 pretreatment on [^{67}Ga]Ac-CG6 accumulation in the blood, AsPC-1,

and MIA PaCa-2 xenografts.

Each column represents an average of 3–4 mice, and each error bar represents the standard

deviation. * indicates $P < 0.05$ (Mann–Whitney U-test).
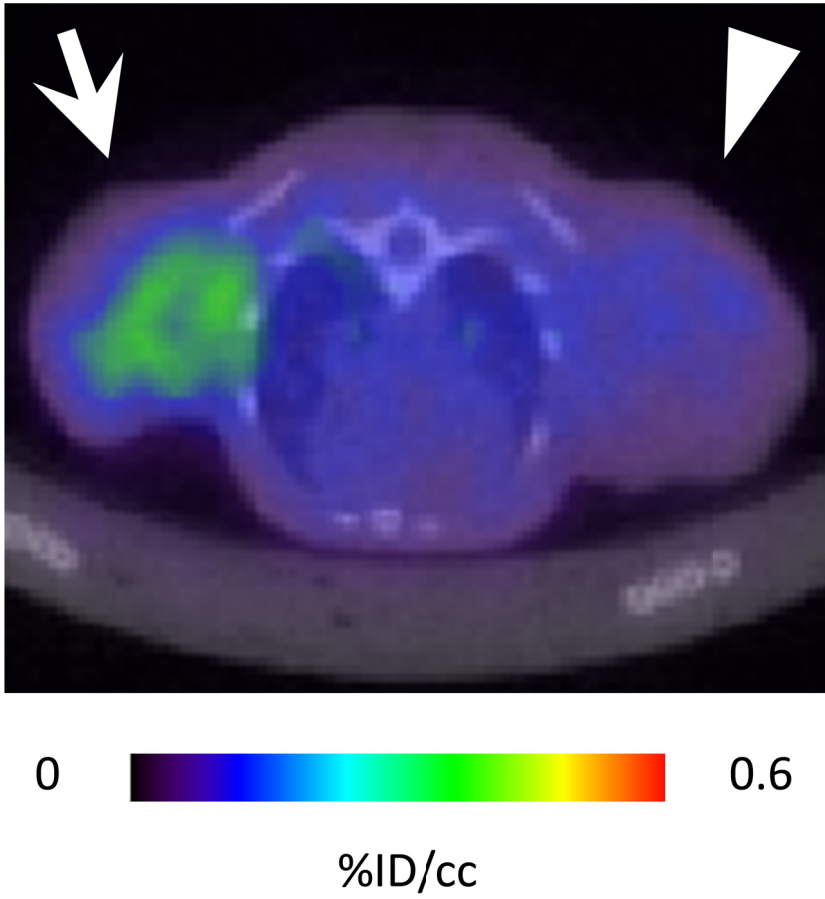
Figure 3

Fig. 3. A representative PET image of an AsPC-1- and MIA PaCa-2-xenografted mouse with

$[^{68}\text{Ga}]$Ac-CG6.

The arrow and arrowhead indicate AsPC-1 and MIA PaCa-2 xenografts, respectively.

Figure 4

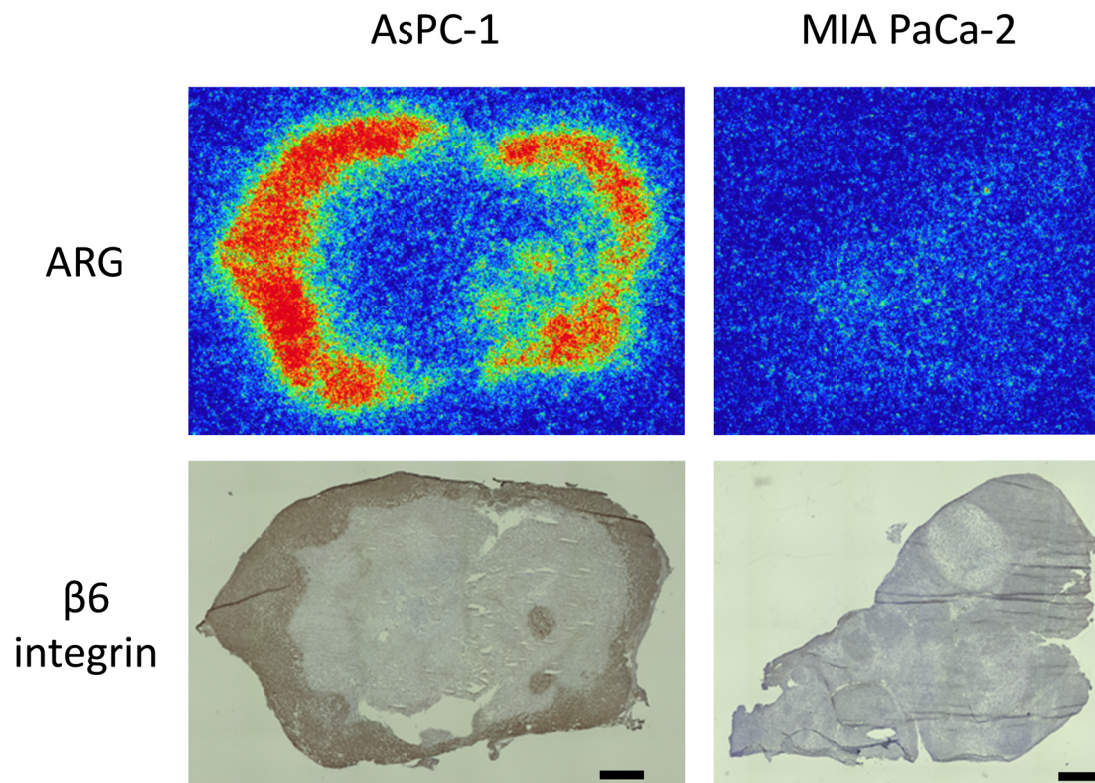**Fig. 4.** Representative images of autoradiograms (ARG) and β6 integrin immunostainings in AsPC-1 and MIA PaCa-2 xenografts.

The expression of β6 integrin is remarkably observable in the marginal regions of the AsPC-1 xenograft and the radioactivity accumulation coincides with those regions. Bars; 1 mm.

Supplementary Material

Table S1. *m/z* values of the peptides

| Peptides	Exact mass	[M+4H]$^{4+}$	
	(M$^+$)	Calcd.	Found
H-Cys(mal-NOTA)-Gly-A20FMDV2-NH$_2$	2747.5	687.9	688.9
H-Cys(mal-NOTA)-Gly4-A20FMDV2-NH$_2$	2918.5	730.6	731.5
H-Cys(mal-NOTA)-Gly6-A20FMDV2-NH$_2$	3032.6	759.2	759.4
Ac-Cys(mal-NOTA)-Gly6-A20FMDV2-NH$_2$	3074.6	769.7	770.3
H-Cys(mal-NOTA)-Gly8-A20FMDV2-NH$_2$	3146.6	787.7	788.7
H-Cys(mal-NOTA-^{nat}Ga)-Gly-A20FMDV2-NH$_2$	2814.4	704.6	705.0
H-Cys(mal-NOTA-^{nat}Ga)-Gly4-A20FMDV2-NH$_2$	2985.4	747.4	747.7
H-Cys(mal-NOTA-^{nat}Ga)-Gly6-A20FMDV2-NH$_2$	3099.5	775.9	776.2
Ac-Cys(mal-NOTA-^{nat}Ga)-Gly6-A20FMDV2-NH$_2$	3141.5	786.4	786.6
H-Cys(mal-NOTA-^{nat}Ga)-Gly8-A20FMDV2-NH$_2$	3213.5	804.4	804.6

Figure S1
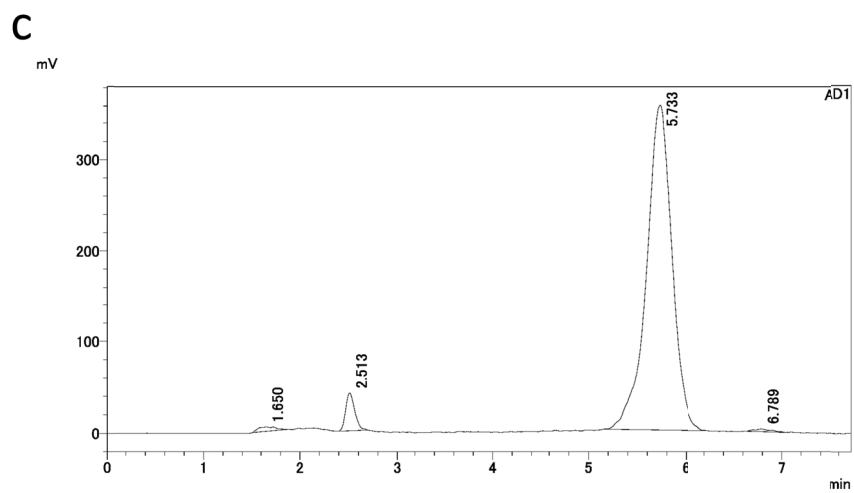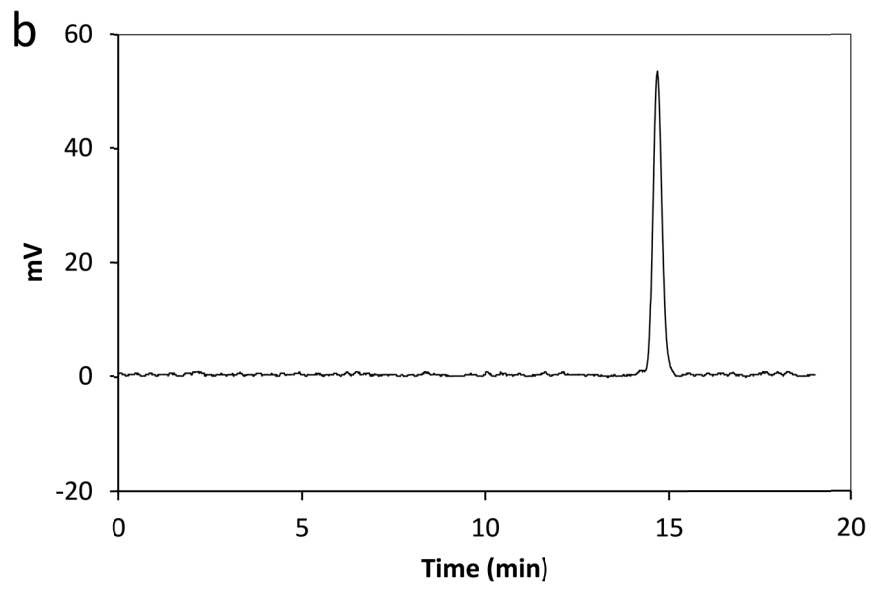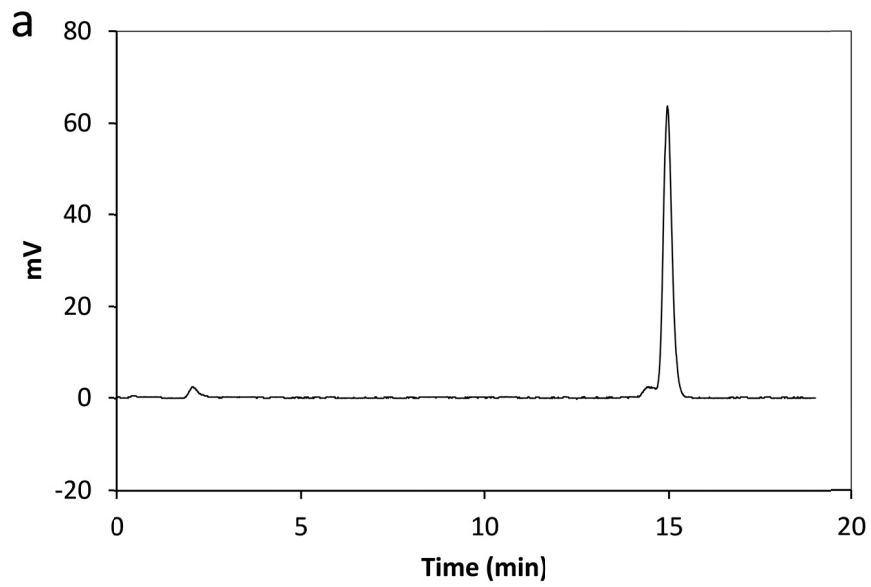
Figure S1. Radiochromatograms of [^{67}Ga]CG6 (a), [^{67}Ga]Ac-CG6 (b), and [^{68}Ga]Ac-CG6 (c).

The retention time of each probe was 14.96 min (a), 14.69 min (b), and 5.733 min (c). The mobile

phase used in (a) and (b) was a linear gradient of 0.1% aqueous trifluoroacetic acid (TFA) and

acetonitrile from 8:2 to 6:4 over 20 min and that used in (c) was 0.1% aqueous TFA:acetonitrile =

73:27.